

**Karim Abdel-Malek
Harn-Jou Yeh**

Center for Computer Aided Design
2129 Engineering Building
Department of Mechanical Engineering
The University of Iowa
Iowa City, IA 52242
Telephone (319) 335-5676
Fax (319) 335-5669
amalek@icaen.uiowa.edu

Analytical Boundary of the Workspace for General 3-DOF Mechanisms

Abstract

An analytical method is presented to obtain all surfaces enveloping the workspace of a general 3-DOF mechanism. The method is applicable to kinematic chains that can be modeled using the Denavit-Hartenberg representation for serial kinematic chains or its modification for closed-loop kinematic chains. The method developed is based upon analytical criteria for determining singular behavior of the mechanism. By manipulating the Jacobian of the underlying mechanism, first-order singularities are computed. These singularities are then substituted into the constraint equation to parameterize singular surfaces representing barriers to motion. Singular surfaces are those resulting from a singular behavior of a joint generalized coordinate, allowing the manipulator to lose one or more degrees of mobility. These surfaces are then intersected to determine singular curves, which represent the manipulator losing at least two degrees of mobility. Difficulties in separating singular behaviors at points along singular curves are encountered. Also, difficulties in computing tangents at the intersections of singular curves are addressed. These difficulties are resolved using an analysis of a quadratic form of the intersection of singular surfaces. An example is presented to validate the theory. Although the methods used are numerical, the main result of this work is the ability to analytically define boundary surfaces of the workspace.

1. Introduction

Analytical criteria for determining workspaces of simple general 3-DOF manipulators were discussed in Abdel-Malek (1994). Difficulties were encountered in using

marching methods for tracing parametric curves of a pair of intersecting singular surfaces and in computing tangents at the intersections of singular curves (bifurcation points). Singular surfaces were shown to be those surfaces representing the manipulator losing one or more degrees of mobility. Singular curves are curves resulting from the intersections of singular surfaces. Although the method is general, difficulties were also encountered in partitioning singular surfaces to a number of subsurfaces. These difficulties are addressed in this article.

Some of the earliest studies on the subject of manipulator performance in terms of workspace were conducted by Vinogradov et al. (1971), where the term "service sphere" was introduced. A study of the relationship between the kinematic geometry and manipulator performance including workspace was presented by Roth (1975). A numerical approach to this problem was formulated and solved by Kumar and Waldron (1981) via tracing boundary surfaces of a workspace. Tsai and Soni (1981) studied accessible regions of planar manipulators, while Gupta and Roth (1982) studied the effect of hand size on workspace analysis. Pennock and Kassner (1993) presented a numerical algorithm for the general study of a planar 3-DOF manipulator.

Recently, Haug et al. (1994) formulated numerical criteria to find the workspace (so-called accessible output set) of a general multi-degree-of-freedom system via the study of a row-rank deficiency of its Jacobian. The algorithm computes tangent vectors at bifurcation points of continuation curves that define the boundary of manipulator workspaces. A cross-section of the workspace is performed, and boundary continuation curves are traced. The method was demonstrated for a closed-loop mechanism called the Stewart Platform (Qiu et al. 1995), where continuation curves are

evaluated on the exterior boundary of the workspace. These curves are then assembled into a mesh that is enveloped by appropriate surface patches. This method has proved efficient for determining the general shape of the workspace. The main difficulty is in determining the status of a singularity at points along continuation curves. Singular behavior occurring at points along the curves is not identified. In addition, this method is completely numerical and does not result in analytical surfaces bounding the workspace. The initial criteria for this computational method were presented by Haug et al. (1992) and Wang and Wu (1993). More recently, an algebraic formulation to determine the workspace of four-revolute manipulators was presented by Cecarelli and Vinciguerra (1995). The benefit of this method is shown in using the ability to determine holes and voids in the workspace.

Since the dexterous workspace is a subspace of the workspace, it is relevant to list some of the works that deal with this area of research. The dexterous workspace of a manipulator as defined by Kumar and Waldron (1980) is a subspace of the workspace within which a vector on the end effector may assume all orientations. Dexterity was also studied by Lai (1986) and Lai and Menq (1988), where the dexterous workspace was theoretically defined for a special case of manipulators with wrists having a full range of orientations. Numerical criteria for mapping *dexterous charts* depicting all possible orientabilities at a target were addressed by Abdel-Malek (1994). Manipulator dexterity was studied by Yang and Lee (1983), Yang and Lai (1985), and Emiris (1993). Studies of workspace and dexterity of parallel manipulators are reported by Agrawal (1990) and Gosselin and Angeles (1990).

The objective of this article is to analytically determine the surfaces enveloping the workspace of a defined point in a 3-DOF mechanism. Difficulties encountered in tracing parametric singular curves resulting from the intersection of two singular surfaces will be addressed. These singular curves will be shown to partition singular surfaces into a number of regions called subsurfaces. Subsurfaces will be shown to exist either entirely inside the workspace, or entirely on the boundary of the workspace. Often times, the intersection of two singular surfaces results in more than one singular curve. These curves may intersect at a point called the bifurcation point. An example is presented in detail to demonstrate the methodology. The method is general, and has been implemented into a computer program.

2. Characterization of Singularities

A constraint equation for a point on a mechanism (with open or closed kinematic chains) can be represented

by writing a kinematic constraint vector function as $\Phi: R^n \rightarrow R^l$ such that the constraint equations are

$$\Phi(\mathbf{q}) = \begin{bmatrix} \Phi_1(q_1, q_2, q_3) \\ \Phi_2(q_1, q_2, q_3) \\ \Phi_3(q_1, q_2, q_3) \end{bmatrix} = \mathbf{0} \quad (1)$$

where $\mathbf{q} = [q_1, q_2, q_3]^T \in R^3$ is the vector of generalized coordinates used to characterize the configuration of each link of the mechanism. For an open kinematic chain, the Denavit-Hartenberg representation method can be used (Denavit and Hartenberg 1955). For multiloop kinematic chains, a modified Denavit-Hartenberg representation method, called the K-K method (Kleininger 1986), can be used. Let the vector \mathbf{x} characterize the position of a point w on the end effector of a manipulator. Then the entire set of points touched by w is defined by

$$\mathbf{x}(\mathbf{q}) = {}^0\mathbf{R}_3(\mathbf{q})^3\mathbf{x}_w + {}^0\mathbf{p}_3(\mathbf{q}) \quad (2)$$

where ${}^3\mathbf{x}_w$ is the vector describing a point resolved in the reference frame of link 3, ${}^0\mathbf{R}_3$ is the rotation matrix between link 0 and link 3, and ${}^0\mathbf{p}_3$ is the position vector from the reference frame to the origin of link 3. For a given configuration of the manipulator, the generalized coordinates satisfy independent holonomic kinematic constraint equations of the form

$$\Phi(\mathbf{q}) = \mathbf{x} - {}^0\mathbf{R}_3^3\mathbf{x}_w - {}^0\mathbf{p}_3 = 0 \quad (3)$$

To impose joint limits of the actuators in terms of the generalized variables, it is possible to transform a constraint of the form

$$q_i^{\min} \leq q_i \leq q_i^{\max} \quad i = 1, 2, 3 \quad (4)$$

into an equation by introducing a new generalized coordinate λ_i , such that the inequality constraint of eq. (4) can be rewritten as

$$q_i = a_i + b_i \sin \lambda_i \quad (5)$$

where $a_i = (q_i^{\max} + q_i^{\min})/2$ and $b_i = (q_i^{\max} - q_i^{\min})/2$ are the midpoint and half-range of the inequality constraint (Haug et al. 1994). Thus each constraint is parameterized as

$$q_1 = b_1 + c_1 \sin \lambda_1 \quad (6a)$$

$$q_2 = b_2 + c_2 \sin \lambda_2 \quad (6b)$$

$$q_3 = b_3 + c_3 \sin \lambda_3 \quad (6c)$$

The combination of three joints, coupled with a mechanism's joint limits, may result in a complex workspace. To analytically find expressions for the boundary surfaces of this set, it is necessary to determine (1) singular surfaces due to first-order singularities associated with the set, (2) singular curves that partition singular surfaces to

subsurfaces, and (3) which of these subsurfaces are on the boundary. When determining singular curves, in many instances it is necessary to compute a multiple of curves, some of which are intersecting. The problem of tracing a multiple of curves is addressed using continuation methods and computing tangents at bifurcation points.

2.1. First-Order Singularities

A first-order singularity defined in the context of this article is the value of a generalized coordinate that makes the Jacobian singular, i.e., that has no inverse if the matrix is square, and is row-rank deficient if the matrix is not square. Singularities defined by μ_i are the generalized coordinates at which the manipulator loses one or more degrees of mobility. First-order singularities commonly fall into two categories (McKerrow 1991):

1. workspace-internal singularities, which occur within the workspace of the manipulator (e.g., when two or more axes line up); and
2. workspace-boundary singularities, which occur at joint limits (e.g., with an arm fully retracted to the inner boundary of the workspace).

First-order singularities are computed by equating the determinant of the Jacobian of the mechanism to zero and then computing the roots. The constraint Jacobian of the constraint function $\Phi(\mathbf{q})$ for a certain configuration \mathbf{q}^0 is the 3×3 matrix

$$\Phi_{\mathbf{q}}(\mathbf{q}^0) = \left[\frac{\partial \Phi_i}{\partial q_j}(\mathbf{q}^0) \right] \quad (7)$$

For systems with more than three degrees of freedom, this condition can be broadened to a row-rank deficiency of the Jacobian, since it is not square. The Jacobian with respect to the new coordinates $\lambda = [\lambda_1 \lambda_2 \lambda_3]$ can be written as

$$\Phi_{\lambda} = \frac{\partial \Phi_i}{\partial q_j} \frac{\partial q_j}{\partial \lambda_j} = \Phi_{\mathbf{q}} \mathbf{q}_{\lambda} \quad (8)$$

Singularities are determined by equating the determinant of Φ_{λ} to zero such that

$$\mathbf{F}(\lambda) = |\Phi_{\mathbf{q}} \mathbf{q}_{\lambda}| = 0 \quad (9)$$

When substituting a value for one of the generalized coordinates in the constraint equation, the resulting function describes a parametric surface (two parameters) called a singular surface. To parameterize singular surfaces, first-order singularities are substituted into the constraint equation. Determining the roots of $\mathbf{F}(\lambda)$ and substituting the results into eq. (2), a set of first-order singularities $\mu_i (i = 1, \dots, m)$ is generated, where μ_i is the generalized coordinate consistent with the roots of $\mathbf{F}(\lambda) = 0$, and m is the total number of singularities.

Substituting each singularity into eq. (2) results in a set of parameterized singular surfaces $X^i(\mu_i)$ such that

$$X^i(\mu_i) = [\mathbf{x}^1(\mu_i), \mathbf{x}^2(\mu_i), \dots, \mathbf{x}^m(\mu_i)] \quad (10)$$

where $i = 1, \dots, m$. Singular surfaces are two-dimensional in three-dimensional space, generated by having one of the generalized coordinates be a constant (a singularity).

2.2. Second-Order Singularities

Singular surfaces generated by eq. (10) are barriers to end-effector motion. These surfaces may exist inside the workspace, on the outer surface, or they may extend to be both internal and external to the workspace. Singular surfaces may intersect each other, resulting in intersection curves called singular curves. These curves between singular surfaces determine a different type of singularity, which divides a singular surface into a number of subsurfaces. The set of generalized coordinates (two constant generalized coordinates) resulting from this intersection are called second-order singularities. In the analysis that follows, it will be necessary to determine these curves and their intersections. It will not be necessary, however, to determine the value of the second-order singularity. Pairs of surfaces are intersected such that

$$\mathbf{x}^i(\mu_i) - \mathbf{x}^j(\mu_j) = 0 \quad \text{for } i \neq j \quad (11)$$

These surfaces can be written in terms of their respective parameters. For example, if $\mu_i = q_3^0$ then $\mathbf{x}^i(\mu_i)$ is parameterized as $\mathbf{x}^i(q_1, q_2)$, and if $\mu_j = q_1^0$ then $\mathbf{x}^j(\mu_j)$ is parameterized as $\mathbf{x}^j(q_2, q_3)$. Eq. (11) can be rewritten as

$$\mathbf{x}^i(q_1, q_2) - \mathbf{x}^j(q_2, q_3) = \mathbf{0} \quad (12)$$

and to eliminate any confusion, the parameters q_2 and q_3 in $\mathbf{x}^j(q_2, q_3)$ are replaced by t_1 and t_2 such that

$$\mathbf{x}^i(q_1, q_2) - \mathbf{x}^j(t_1, t_2) = \mathbf{0} \quad (13)$$

The problem of numerically determining the intersection curve is complicated when several curves exist. In many cases, singular surfaces are parameterically similar (e.g., two perpendicular intersecting cylindrical surfaces of equal radii will result in two intersection curves). In addition, most numerical algorithms require the estimation of a starting point on or close to the solution curve. Muellenheim (1991) has presented an iterative method for calculating a starting point which is close to a solution curve. Wilf and Manor (1993) have presented a method using a modification of Levin's ruled-surface parameterization scheme, guided by invariant-factors classification and, furthermore, by factorization of the parameterization

polynomials. In this article, the Moore-Penrose pseudo-inverse is used to estimate an initial point on a curve of intersection.

The curve is traced using a marching method (Pratt and Geisow 1986). The algorithm requires a vector-tangent direction to compute marching parameters. These numerical methods, however, do not address the status of higher-order singularities at bifurcation points. The problem of determining the behavior at singular points will be shown to reduce to a study of the system's eigenvalues by studying the curve's curvature. The eigenvectors are then the tangent directions at a bifurcation point.

We are seeking solutions to the intersection of two singular surfaces $\mathbf{x}^1(q_1, q_2)$ and $\mathbf{x}^2(u_1, u_2)$ subject to inequality constraints, such that a constraint function of eq. (3) can be augmented as

$$\mathbf{H}(\mathbf{s}) = \begin{bmatrix} \mathbf{x}^1(q_1, q_2) - \mathbf{x}^2(t_1, t_2) \\ q_1 - a_1 - a_2 \sin \lambda_1 \\ q_2 - b_1 - b_2 \sin \lambda_2 \\ t_1 - c_1 - c_2 \sin \lambda_3 \\ t_2 - d_1 - d_2 \sin \lambda_4 \end{bmatrix} = \mathbf{0} \quad (14)$$

where \mathbf{s} is the extended vector defined as $\mathbf{s} = [q_1 \ q_2 \ t_1 \ t_2 \ \lambda_1 \ \lambda_2 \ \lambda_3 \ \lambda_4]^T$. Since the Jacobian of $\mathbf{H}(\mathbf{s})$ is not square, the problem of obtaining an initial solution can be solved using the Moore-Penrose pseudo-inverse (Allgower and Georg 1990). The new generalized coordinates are calculated by evaluating

$$\Delta \mathbf{s} = \mathbf{H}_s^* (-\mathbf{H}) \quad (15)$$

where \mathbf{H}_s^* is the Moore-Penrose pseudo-inverse of the Jacobian $\mathbf{H}_s = [\partial H_i / \partial s_j]$, defined by

$$\mathbf{H}_s^* = \mathbf{H}_s^T (\mathbf{H}_s \mathbf{H}_s^T)^{-1} \quad (16)$$

This method converges within a few iterations without adding any new constraints (Allgower and Georg 1990). Once a starting point is found, the intersection curve is traced along the tangent direction by using the so-called marching method (Pratt and Geisow 1986). The tangent vector at the starting point can be computed by calculating the cross-product of two normal vectors. At a known point on the surface $\mathbf{x}^1(q_1, q_2)$, there are two linearly independent tangents which are the derivatives of the surface with respect to its parameters. Let $\mathbf{x}_{q_1}^1$ denote the derivative of \mathbf{x}^1 with respect to q_1 , and $\mathbf{x}_{q_2}^1$ denote the derivative of \mathbf{x}^1 with respect to q_2 . The cross-product of these vectors results in a normal to the surface such that

$$\mathbf{n}^1 = (\mathbf{x}_{q_1}^1 \times \mathbf{x}_{q_2}^1) / \|\mathbf{x}_{q_1}^1 \times \mathbf{x}_{q_2}^1\| \quad (17)$$

Similarly, the second surface has a normal such that

$$\mathbf{n}^2 = (\mathbf{x}_{q_2}^2 \times \mathbf{x}_{q_3}^2) / \|\mathbf{x}_{q_2}^2 \times \mathbf{x}_{q_3}^2\| \quad (18)$$

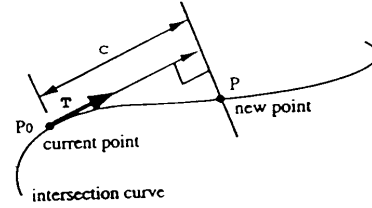


Fig. 1. Geometric interpretation of the step-marching procedure.

and the tangent τ is computed as

$$\tau = \mathbf{n}^1 \times \mathbf{n}^2 \quad (19)$$

The new step-constraint equation can be written as

$$[\mathbf{x}^1(q_1, q_2) - \mathbf{x}^0] \cdot \tau - c = 0 \quad (20)$$

where \mathbf{x}^0 is the computed point, and c is the step-size. The geometric interpretation of the step-marching procedure is shown in Fig. 1.

Although this method will converge, it is possible to find only one starting point, and thus only one corresponding branch of intersection will be traced. To determine other intersection branches, it is necessary to study singular behavior along the curve. Allgower and Georg (1990) suggest monitoring the curve for a change in sign of the following determinant

$$\det \begin{pmatrix} \mathbf{H}_q \mathbf{c}(\sigma) \\ \dot{\mathbf{c}}(\sigma) \end{pmatrix} \quad (21)$$

where $\mathbf{c}(\sigma)$ is the curve of intersection, $\dot{\mathbf{c}}(\sigma)$ is the tangent, and σ is the arc length. Thus, to recognize that a singularity has occurred, eq. (21) is used with a diminishing-step variable until the singular point is computed. To trace the second curve, it is necessary to compute the second tangent at this bifurcation point. For this reason, it is assumed that the surfaces are tangent at the bifurcation point such that

$$\mathbf{x}_{q_1}^1 \times \mathbf{x}_{q_2}^1 // \mathbf{x}_{t_1}^2 \times \mathbf{x}_{t_2}^2 \neq \mathbf{0} \quad (22)$$

The normal can be determined from

$$\mathbf{n} = \frac{\mathbf{x}_{q_1}^1 \times \mathbf{x}_{q_2}^1}{\|\mathbf{x}_{q_1}^1 \times \mathbf{x}_{q_2}^1\|} \quad (23)$$

Lucaks (1990) showed that a branch of a curve can be parameterized in terms of its arc length σ such that

$$\mathbf{r}(\sigma) = \mathbf{x}^1(q_1(\sigma), q_2(\sigma)) = \mathbf{x}^2(t_1(\sigma), t_2(\sigma)) \quad (24)$$

Taking the derivative of both sides of eq. (24) with respect to σ yields the tangent vector

$$\frac{\partial \mathbf{r}}{\partial \sigma} = \mathbf{x}_{q_1}^1(q_1)_\sigma + \mathbf{x}_{q_2}^1(q_2)_\sigma = \mathbf{x}_{t_1}^2(t_1)_\sigma + \mathbf{x}_{t_2}^2(t_2)_\sigma \quad (25)$$

Multiplying vectorially by $\mathbf{x}_{q_1}^1$, we get

$$(\mathbf{x}_{q_1}^1 \times \mathbf{x}_{q_2}^1) \cdot (q_2)_\sigma = (\mathbf{x}_{q_1}^1 \times \mathbf{x}_{t_1}^2) \cdot (t_1)_\sigma + (\mathbf{x}_{q_1}^1 \times \mathbf{x}_{t_2}^2) \cdot (t_2)_\sigma \quad (26)$$

Dividing by $\mathbf{x}_{q_1}^1 \times \mathbf{x}_{q_2}^1$ yields

$$(t_1)_\sigma = \alpha(q_1)_\sigma + \beta(q_2)_\sigma \quad (27)$$

$$(t_2)_\sigma = \gamma(q_1)_\sigma + \delta(q_2)_\sigma \quad (28)$$

where

$$\alpha\delta - \beta\gamma \neq 0 \quad (29)$$

Derive both sides of eqs. (25) and (26) to yield

$$\mathbf{x}_{q_1 q_2}^1 [(q_1)_\sigma]^2 + 2\mathbf{x}_{q_1 q_2}^1 (q_1)_\sigma (q_2)_\sigma + \mathbf{x}_{q_2 q_2}^1 [(q_2)_\sigma]^2 + \mathbf{x}_{q_1}^1 (q_1)_{\sigma\sigma} + \mathbf{x}_{q_2}^1 (q_2)_{\sigma\sigma} = \quad (30)$$

$$\mathbf{x}_{t_1 t_1}^2 [(t_1)_\sigma]^2 + 2\mathbf{x}_{t_1 t_2}^2 (t_1)_\sigma (t_2)_\sigma + \mathbf{x}_{t_2 t_2}^2 [(t_2)_\sigma]^2 + \mathbf{x}_{t_2}^2 (t_2)_{\sigma\sigma} + \mathbf{x}_{t_1}^2 (t_1)_{\sigma\sigma} \quad (31)$$

Using the dot product of \mathbf{n} in both sides of eqs. (30) and (31) yields

$$\langle \mathbf{x}_{q_1 q_1}^1, \mathbf{n} \rangle [(q_1)_\sigma]^2 + 2 \langle \mathbf{x}_{q_1 q_2}^1, \mathbf{n} \rangle (q_1)_\sigma (q_2)_\sigma + \langle \mathbf{x}_{q_2 q_2}^1, \mathbf{n} \rangle [(q_2)_\sigma]^2 = \quad (32)$$

$$\langle \mathbf{x}_{t_1 t_1}^2, \mathbf{n} \rangle [(t_1)_\sigma]^2 + 2 \langle \mathbf{x}_{t_1 t_2}^2, \mathbf{n} \rangle (t_1)_\sigma (t_2)_\sigma + \langle \mathbf{x}_{t_2 t_2}^2, \mathbf{n} \rangle [(t_2)_\sigma]^2 \quad (33)$$

The normal curvatures on both sides are realized. Substituting eqs. (27) and (28) into eqs. (32) and (33) yields the following relation:

$$\theta[(q_1)_\sigma]^2 + 2\mu(q_1)_\sigma(q_2)_\sigma + \kappa[(q_2)_\sigma]^2 = 0 \quad (34)$$

which is a quadratic form that can be written as

$$[(q_1)_\sigma \quad (q_2)_\sigma] \begin{bmatrix} \theta & \mu \\ \mu & \kappa \end{bmatrix} \begin{bmatrix} (q_1)_\sigma \\ (q_2)_\sigma \end{bmatrix} = 0 \quad (35)$$

Define the matrix Λ such that

$$\Lambda = \begin{bmatrix} \theta & \mu \\ \mu & \kappa \end{bmatrix} \quad (36)$$

then the eigenvalues are computed as

$$\lambda_1 = \frac{\theta + \kappa}{2} + \sqrt{\left(\frac{\theta - \kappa}{2}\right)^2 + \mu^2} \quad (37)$$

$$\lambda_2 = \frac{\theta + \kappa}{2} - \sqrt{\left(\frac{\theta - \kappa}{2}\right)^2 + \mu^2} \quad (38)$$

Therefore the solution in the neighborhood of a singular point depends on the definiteness of the quadratic form defined by eq. (35). Furthermore, the two vectors defining the tangent directions are the corresponding eigenvectors.

Vectors in the tangent directions \mathbf{v}_1 and \mathbf{v}_2 are determined such that

$$\boldsymbol{\tau}_1 = \sqrt{-\lambda_2} \mathbf{v}_1 + \sqrt{\lambda_1} \mathbf{v}_2 \quad (39)$$

$$\boldsymbol{\tau}_2 = \sqrt{-\lambda_2} \mathbf{v}_1 - \sqrt{\lambda_1} \mathbf{v}_2 \quad (40)$$

To determine the singularity along the traced curve, Lucaks (1990) presented, without proof, that four cases exist, which depend on the behavior of the quadratic form of eq. (35):

1. the point is isolated if the form is definite, $(\lambda_1 \cdot \lambda_2) > 0$;
2. the point is a bifurcation point (two branches) if the form is indefinite, $(\lambda_1 \cdot \lambda_2) < 0$;
3. one branch passes through the point if the form is semidefinite, $\lambda_1 = 0$ or $\lambda_2 = 0$, but not both; and
4. a second-order singularity exists at the point if the form is zero, or both $\lambda_1 = 0$ and $\lambda_2 = 0$.

The physical significance of these singular curves stems from having two constant generalized coordinates, i.e., the resulting curve is one-dimensional in three-dimensional space. These singular curves partition singular surfaces into a number of regions called subsurfaces that are denoted by Ψ^i . For a singular surface, the intersection of curves c^k results in nodes n^j . For example, to determine subsurfaces on surface \mathbf{x}^3 in Fig. (2a), \mathbf{x}^3 is intersected with \mathbf{x}^2 and \mathbf{x}^1 to obtain singular curves. The singular curves are superimposed on surface \mathbf{x}^3 as depicted in Fig. (2b). The curves partition this surface to four subsurfaces, each of which is bounded by curve segments. Subsurface Ψ^4 , for example, is bound by curve segments c^3 between nodes n^2 and n^3 , curve segment c^2 between nodes n^3 and n^1 , and curve segment c^1 between nodes n^1 and n^3 .

The matrix of subsurfaces is

$$\Psi^i(\mu_i) = [\Psi^1(\mu_1), \Psi^2(\mu_2), \dots, \Psi^m(\mu_m), \Psi^m(\mu_{m+1}), \dots, \Psi^n(\mu_n)] \quad (41)$$

Eq. (41) includes all subsurfaces due to internal, boundary, and higher-order singularities. It remains to determine whether these subsurfaces are internal or boundary surfaces. This can be performed by perturbing a known point on the subsurface and determining whether this point satisfies the equation of constraint, eq. (3), subject to inequality constraints of eq. (6). We have not found an efficient method for determining this point. Any point can be chosen, provided that it is not on the boundary. For subsurface $\Psi^i(\mathbf{q})$, the partial derivatives with respect to the parameterization variables q_1 and q_2 are $\frac{\partial \Psi^i}{\partial q_1}$ and $\frac{\partial \Psi^i}{\partial q_2}$. At any regular point \mathbf{q}^0 on the subsurface, these vectors are linearly independent and tangent to the coordinate curves through \mathbf{q}^0 (they span the tangent plane of $\Psi^i(\mathbf{q})$).

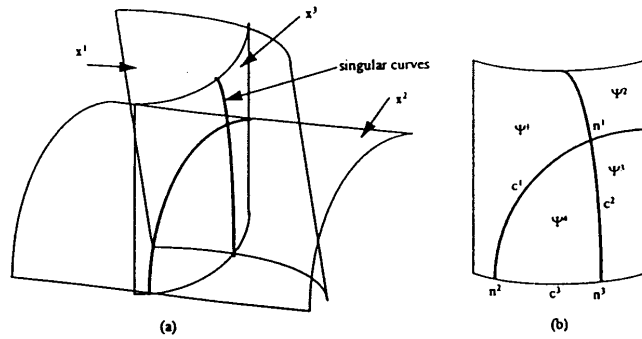


Fig. 2. (A) Intersection of singular surfaces. (B) Partitioning of a singular surface to subsurfaces.

at \mathbf{q}^0). The unit vector $\hat{\mathbf{n}}$, which is orthogonal to those vectors, is

$$\hat{\mathbf{n}}(\mathbf{q}^0) = \frac{\left(\frac{\partial \Psi^i}{\partial q_1} \times \frac{\partial \Psi^i}{\partial q_2} \right)}{\left\| \frac{\partial \Psi^i}{\partial q_1} \times \frac{\partial \Psi^i}{\partial q_2} \right\|} \quad (42)$$

For a small perturbation $\partial \varepsilon$ about the point \mathbf{q}^0 and along the normal $\hat{\mathbf{n}}(\mathbf{q}^0)$, the coordinates of the perturbed point are

$$\mathbf{x} = \Psi^i(\mathbf{q}^0) \pm \partial \varepsilon \hat{\mathbf{n}}(\mathbf{q}^0) \quad (43)$$

For the perturbed point to exist inside the workspace, it must satisfy eq. (3), subject to inequality constraints of eq. (6). Thus, a solution is sought to the following system of equations:

$${}^0\mathbf{R}_3^3 \mathbf{x}_w + {}^0\mathbf{p}_3 - \Psi^i(\mathbf{q}^0) \mp \partial \varepsilon \hat{\mathbf{n}}(\mathbf{q}^0) = \mathbf{0} \quad (44)$$

$$q_1 - b_1 - c_1 \sin \lambda_1 = 0 \quad (45a)$$

$$q_2 - b_2 - c_2 \sin \lambda_2 = 0 \quad (45b)$$

$$q_3 - b_3 - c_3 \sin \lambda_3 = 0 \quad (45c)$$

The subsurface $\Psi^i(\mathbf{q})$ is an internal surface if and only if there exists a solution for eq. (44) for both perturbations $\pm \partial \varepsilon$, consistent with the equalities of eq. (45).

3. A General 3-DOF Mechanism

To illustrate the foregoing analysis, consider the three-degree-of-freedom manipulator depicted in Fig. 3 which has three revolute joints. The boundary surfaces to the workspace generated by the point ${}^0\mathbf{x}_w = [0 \ 0 \ 0]^T$ will be studied.

3.1. Determining First-Order Singularities

For this manipulator, the three homogeneous transformation matrices using the Denavit-Hartenberg representation

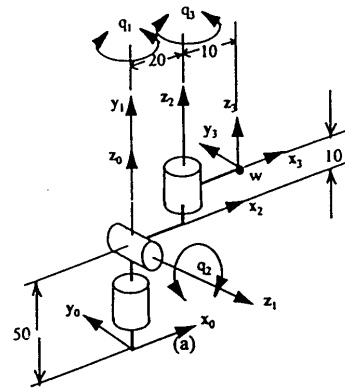


Fig. 3. A 3-DOF manipulator.

of joints 1, 2, and 3 are

$${}^0\mathbf{T}_1 = \begin{bmatrix} \cos q_1 & 0 & \sin q_1 & 0 \\ \sin q_1 & 0 & -\cos q_1 & 0 \\ 0 & 1 & 0 & 50 \\ 0 & 0 & 0 & 1 \end{bmatrix} \quad (46)$$

$${}^1\mathbf{T}_2 = \begin{bmatrix} \cos q_2 & 0 & -\sin q_2 & 20 \cos q_2 \\ \sin q_2 & 0 & \cos q_2 & 20 \sin q_2 \\ 0 & -1 & 0 & 0 \\ 0 & 0 & 0 & 1 \end{bmatrix} \quad (47)$$

$${}^2\mathbf{T}_3 = \begin{bmatrix} \cos q_3 & -\sin q_3 & 0 & 10 \cos q_3 \\ \sin q_3 & \cos q_3 & 0 & 10 \sin q_3 \\ 0 & 0 & 1 & 10 \\ 0 & 0 & 0 & 1 \end{bmatrix} \quad (48)$$

where q_1 , q_2 , and q_3 are the generalized variables representing joint displacements.

Multiplying the matrices $\prod_{i=1}^3 {}^i T_{i-1}$ and extracting the (3×3) rotation matrix yields

$${}^0 R_3 = \begin{bmatrix} \cos q_1 \cos q_2 \cos q_3 & -\cos q_1 \cos q_2 \sin q_3 & & & & \\ -\sin q_1 \sin q_3 & -\sin q_1 \cos q_3 & & & & \\ \sin q_1 \cos q_2 \cos q_3 & -\sin q_1 \cos q_2 \sin q_3 & & & & \\ +\cos q_1 \sin q_3 & +\cos q_1 \cos q_3 & & & & \\ \sin q_2 \cos q_3 & -\sin q_2 \sin q_3 & & & & \\ & & -\cos q_1 \sin q_2 & & & \\ & & -\sin q_1 \sin q_2 & & & \\ & & & \cos q_2 & & \end{bmatrix} \quad (49)$$

The position vector is

$${}^0 x_3 = \begin{bmatrix} 10 \cos q_1 \cos q_2 \cos q_3 - 10 \sin q_1 \sin q_3 \\ -10 \cos q_1 \sin q_2 + 20 \cos q_1 \cos q_2 \\ 10 \sin q_1 \cos q_2 \cos q_3 + 10 \cos q_1 \sin q_3 \\ -10 \sin q_1 \sin q_2 + 20 \sin q_1 \cos q_2 \\ 10 \sin q_2 \cos q_3 + 10 \cos q_2 \\ +20 \sin q_2 + 50 \end{bmatrix} \quad (50)$$

For a general point $\mathbf{x} = [x \ y \ z]^T$, the equation of constraint, eq. (3) of this point is

$$\Phi(\mathbf{q}) = \begin{bmatrix} x - 10 \cos q_1 \cos q_2 \cos q_3 \\ +10 \sin q_1 \sin q_3 \\ +10 \cos q_1 \sin q_2 \\ -20 \cos q_1 \cos q_2 \\ y - 10 \sin q_1 \cos q_2 \cos q_3 \\ -10 \cos q_1 \sin q_3 \\ +10 \sin q_1 \sin q_2 \\ -20 \sin q_1 \cos q_2 \\ z - 10 \sin q_2 \cos q_3 \\ -10 \cos q_2 \\ -20 \sin q_2 - 50 \end{bmatrix} = \mathbf{0} \quad (51)$$

subject to the following joint limits

$$-\frac{\pi}{4} \leq q_1 \leq \frac{5\pi}{4} \quad (52)$$

which is parameterized as

$$q_1 = b_1 + c_1 \sin \lambda_1 = \frac{\pi}{2} + \frac{3\pi}{4} \sin \lambda_1 \quad (53)$$

The second generalized coordinate has limits as

$$-\frac{\pi}{4} \leq q_2 \leq \frac{\pi}{2} \quad (54)$$

and is parameterized as

$$q_2 = b_2 + c_2 \sin \lambda_2 = \frac{\pi}{8} + \frac{3\pi}{8} \sin \lambda_2 \quad (55)$$

The third generalized coordinate has limits

$$0 \leq q_3 \leq 2\pi \quad (56)$$

and is parameterized as

$$q_3 = b_3 + c_3 \sin \lambda_3 = \pi + \pi \sin \lambda_3 \quad (57)$$

To evaluate the Jacobian with respect to the new generalized coordinates λ_i , the matrices $\Phi_{\mathbf{q}}$ and \mathbf{q}_{λ} are evaluated such that

$$\Phi_{\mathbf{q}} = \begin{bmatrix} -10 \sin q_1 \cos q_2 \cos q_3 & -10 \cos q_1 \sin q_2 \cos q_3 \\ -10 \cos q_1 \sin q_3 & -10 \cos q_1 \cos q_2 \\ +10 \sin q_1 \sin q_2 & -20 \cos q_1 \sin q_2 \\ -20 \sin q_1 \cos q_2 & \\ 10 \cos q_1 \cos q_2 \cos q_3 & -10 \sin q_1 \sin q_2 \cos q_3 \\ -10 \sin q_1 \sin q_3 & -10 \sin q_1 \cos q_2 \\ -10 \cos q_1 \sin q_2 & -20 \sin q_1 \sin q_2 \\ +20 \cos q_1 \cos q_2 & \\ 0 & 10 \cos q_2 \cos q_3 \\ & -10 \sin q_2 \\ & +20 \cos q_2 \\ & -10 \cos q_1 \cos q_2 \sin q_3 \\ & -10 \sin q_1 \cos q_3 \\ & -10 \sin q_1 \cos q_2 \sin q_3 \\ & +10 \cos q_1 \cos q_3 \\ & -10 \sin q_2 \sin q_3 \end{bmatrix} \quad (58a)$$

and

$$\mathbf{q}_{\lambda} = \begin{bmatrix} \frac{3\pi}{4} \cos \lambda_1 & 0 & 0 \\ 0 & \frac{3\pi}{8} \cos \lambda_2 & 0 \\ 0 & 0 & \pi \cos \lambda_3 \end{bmatrix} \quad (58b)$$

Internal and boundary singularities are computed by evaluating the determinant of the Jacobian and equating to zero:

$$|\Phi_{\mathbf{q}} \mathbf{q}_{\lambda}| = 1125(-1)^{7/8} \cos \lambda_1 \cos \lambda_2 \cos \lambda_3 [\pi \sin \lambda_3] \\ + (-4 + 2(-1)^{1/2}) [(-1)^{1/4} + 1] \cos \left(\frac{3\pi \sin \lambda_2}{8} \right) \\ + (1 + (-1)^{1/4}) \cos \left(\frac{3 \sin \lambda_2 - 8 \sin \lambda_3}{8} \right) \\ + (1 + (-1)^{1/4}) \cos \left(\frac{3\pi \sin \lambda_2}{8} + \pi \sin \lambda_3 \right) \\ + (2 + 4(-1)^{1/2}) (1 + (-1)^{1/4}) \sin \left(\frac{3\pi \sin \lambda_2}{8} \right) \\ - ((-1)^{1/2} - (-1)^{3/4}) \left[\sin \left(\frac{3 \sin \lambda_2 - 8 \sin \lambda_3}{8} \right) \right. \\ \left. + \sin \left(\frac{3\pi \sin \lambda_2}{8} + \pi \sin \lambda_3 \right) \right] = 0 \quad (59)$$

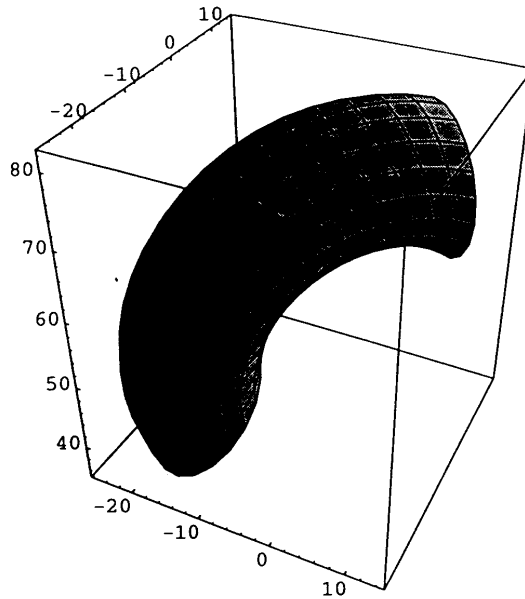


Fig. 4. The singular surface $\mathbf{x}^1(q_2, q_3)$ due to the singularity $q_1 = -\pi/4$.

subject to the inequalities of eqs. (53), (55), and (57). Singularities are determined by finding the roots of eq. (59). For example, the term $\cos \lambda_1$ vanishes if $\lambda_1 = \pi/2$ or $\lambda_1 = -\pi/2$. Substituting λ_1 into eq. (53) results in $q_1 = -\pi/4$ or $q_1 = \pi/4$. The other computed singularities are $q_3 = 0, q_3 = \pi, q_3 = 2\pi, q_2 = -\pi/4$, and $q_2 = \pi/2$. The total number of first-order singularities is seven. The singularity $q_3 = \pi$, however, is inside the interval $[0 \ 2\pi]$. Since both of the endpoints are singularities, $q_3 = \pi$ will not be considered. Singular surfaces are parameterized by substituting each singularity into eq. (50). Note, however, that some of these surfaces are boundary to the workspace, other surfaces are internal, and some surfaces have parts that are on the boundary and parts that are internal. For example, substituting the singularity $q_1 = -\pi/4$ into eq. (50) yields the singular surface parameterized as follows

$$\mathbf{x}^1(q_2, q_3) = \begin{bmatrix} 7.0711 \cos q_2 \cos q_3 \\ +7.0711(\sin q_3 - \sin q_2) \\ +14.1421 \cos q_2 \\ -7.0711 \cos q_2 \cos q_3 \\ +7.0711(\sin q_3 + \sin q_2) \\ -14.1421 \cos q_2 \\ 10 \cos q_3 \sin q_2 \\ +10 \cos q_2 \\ +20 \sin q_2 + 50 \end{bmatrix} \quad (60)$$

with inequality constraints defined as

$$0 \leq q_3 \leq 2\pi \quad (61)$$

$$-0.785 \leq q_2 \leq 1.57 \quad (62)$$

This singular surface $\mathbf{x}^1(q_2, q_3)$ is shown in Figure 4.

Substituting the singularity $q_1 = \pi/4$ yields the surface

$$\mathbf{x}^2(q_2, q_3) = \begin{bmatrix} -7.0711 \cos q_3 \cos q_2 \\ +7.0711(\sin q_3 + \sin q_2) \\ -14.1421 \cos q_2 \\ -7.0711 \cos q_3 \cos q_2 \\ -7.0711(\sin q_3 - \sin q_2) \\ -14.1421 \cos q_2 \\ 10 \cos q_3 \sin q_2 \\ +10 \cos q_2 \\ +20 \sin q_2 + 50 \end{bmatrix} \quad (63)$$

with inequality constraints as

$$0 \leq q_3 \leq 2\pi \quad (64)$$

$$-0.785 \leq q_2 \leq 1.57 \quad (65)$$

The singular surface $\mathbf{x}^2(q_2, q_3)$ is shown in Figure 5. Singular surfaces due to the other singularities are depicted in Figure 6, a, b, c, and d.

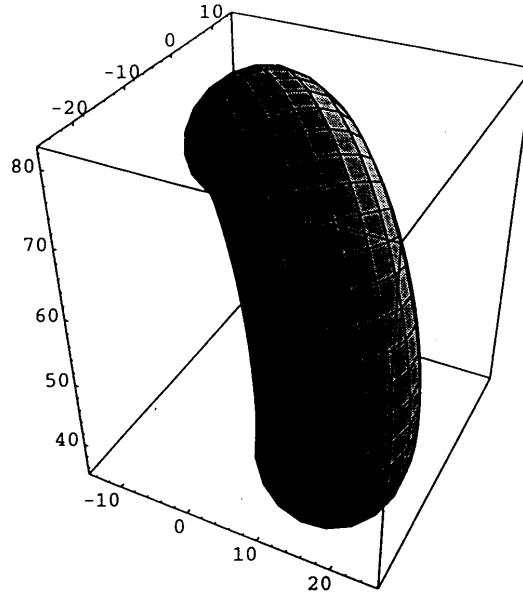


Fig. 5. The singular surface $\mathbf{x}^2(q_2, q_3)$ due to the singularity $q_1 = 5\pi/4$.

3.2. Determining Second-Order Singularities

To determine boundary surfaces to the workspace, it is first necessary to divide singular surfaces into sub-surfaces, and then identify those sub-surfaces that are boundary to the workspace. Singular surfaces are divided into sub-surfaces by computing the curves of intersection between them. Once these curves are determined and each is projected onto its respective parametric space of two variables, each region representing a sub-surface is studied for existence on the boundary of the workspace. To illustrate the determination of sub-surfaces, consider the intersection of the two surfaces $\mathbf{x}^1(q_2, q_3)$ and $\mathbf{x}^2(q_2, q_3)$. The parameters of the second surface will be changed to t_1 and t_2 such that $t_1 = q_2$ and $t_2 = q_3$. The marching method presented in the previous sections is used. The constraint matrix, eq. (14), can be written as

$$\mathbf{H}(\mathbf{q}) = \begin{bmatrix} \mathbf{x}^1(q_2, q_3) - \mathbf{x}^2(t_1, t_2) \\ q_2 - \frac{\pi}{2} - \frac{3\pi}{4} \sin \lambda_1 \\ q_3 - \frac{\pi}{8} - \frac{3\pi}{8} \sin \lambda_2 \\ t_1 - \frac{\pi}{2} - \frac{3\pi}{4} \sin \lambda_3 \\ t_2 - \frac{\pi}{8} - \frac{3\pi}{8} \sin \lambda_4 \end{bmatrix} = \mathbf{0} \quad (66)$$

The starting point, \mathbf{s}^* , computed using the Moore-Penrose pseudo-inverse, is

$$\mathbf{s}^* = [0.6184 \quad 3.4086 \quad 0.6184 \quad 2.8745 \quad 0.1928 \\ 0.0851 \quad 0.1928 \quad -0.0851]$$

Using \mathbf{s}^* as a starting point for the algorithm for mapping marching curves, a singular bifurcation point \mathbf{s}^o , is encountered at

$$\mathbf{s}^o = [0.7854 \quad 3.1416 \quad 0.7854 \quad 3.1416 \quad 0.3398 \\ 0.8306 \times 10^{-9} \quad 0.3398 \quad -0.8306 \times 10^{-9}]$$

The matrix of the quadratic equation, eq. (35) is computed as

$$\Lambda = \begin{bmatrix} \theta & \mu \\ \mu & \kappa \end{bmatrix} = \begin{bmatrix} 14.1421 & 0.6830 \\ 0.6830 & -28.2843 \end{bmatrix} \quad (67)$$

The eigenvalues of the quadratic equation are $\lambda_1 = 14.1421$ and $\lambda_2 = -28.2843$. The first eigenvector due to the first eigenvalue is $\mathbf{v}_1 = [1.0000 \quad 0.16099 \times 10^{-8}]^T$, while the second eigenvector due to the second eigenvalue is $\mathbf{v}_2 = [-0.16099 \times 10^{-8} \quad 1.0000]^T$. To compute the tangents at the bifurcation point, a combination of the eigenvectors is used such that

$$\boldsymbol{\tau}^1 = \sqrt{-\lambda_2} \mathbf{v}_1 + \sqrt{\lambda_1} \mathbf{v}_2 = [5.3182 \quad -3.7606]^T \quad (68)$$

$$\boldsymbol{\tau}^2 = \sqrt{-\lambda_2} \mathbf{v}_1 - \sqrt{\lambda_1} \mathbf{v}_2 = [5.3182 \quad 3.7606]^T \quad (69)$$

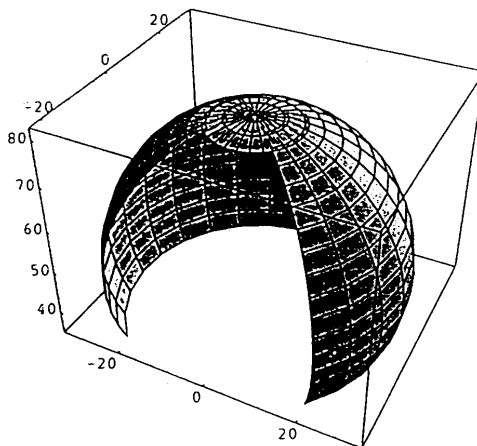
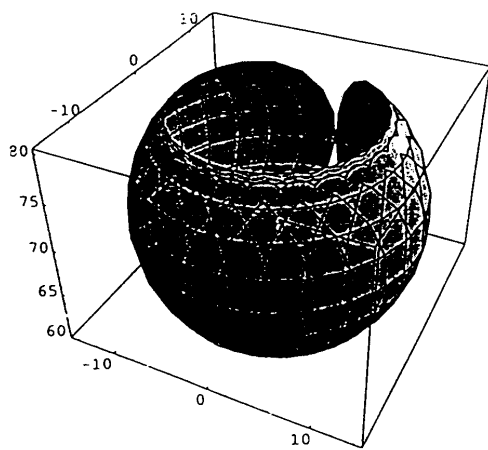
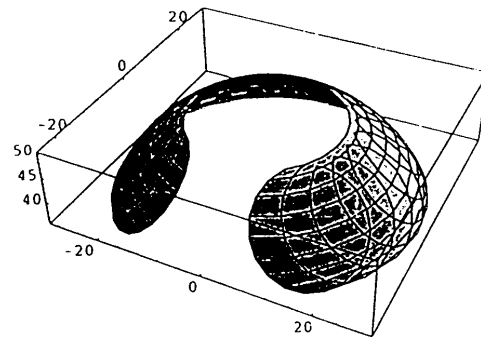
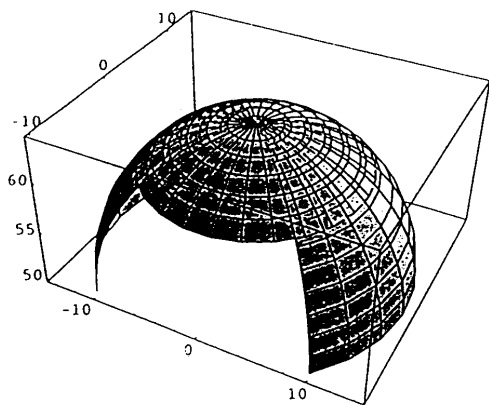


Fig. 6. Singular surfaces due to first-order singularities.

The normalized tangents computed in the parametric space at the bifurcation point are $\tau^1 = [0.8165 \ 0.5773]^T$ and $\tau^2 = [0.8165 \ -0.5774]^T$. The resulting intersecting curves in the parametric space are depicted in Figure 7a, and on the surfaces in Figure 7b.

In addition to the intersection curves resulting from the intersection between $\mathbf{x}^1(q_2, q_3)$ and $\mathbf{x}^2(q_2, q_3)$, surface $\mathbf{x}^1(q_2, q_3)$ intersects with other singular surfaces. The computed intersection curves due to other singular surfaces are superpositioned in Figure 8. These four singular curves (c^1, c^2, c^3 , and c^4) partition surface \mathbf{x}^1 into 12 sub-surfaces.

To determine which subsurface is inside the workspace and which is on the boundary, it is necessary to identify a point that is on the subsurface and use the perturbation technique. Given a number of intersection curves in the parametric space (Figure 8), an algorithm is used to determine the boundary curves of each subsurface. Each pair of intersection curves is intersected to determine intersection points called nodes, which are shown as n^1, n^2, \dots, n^i . Starting at a known point p^0 in the parametric space, a ray is cast in a random direction until this ray intersects a curve (e.g., curve c^1 in Figure 9) to find the initial point κ . On the curve c^1 there are two nodes that are close to κ . Two vectors from the point p^0 are extended to each of the nodes n^1 and n^2 such that $\mathbf{r}^1 = n^1 - p^0$ and $\mathbf{r}^2 = n^2 - p^0$. A vector from p^0 to κ is also formed such that $\mathbf{r} = \kappa - p^0$.

To form a closed boundary of the subsurface, a convention is used such that the normal to the surface, resulting from a cross-product of two vectors, is always positive (rotating counterclockwise). This is the node that results when a positive normal is chosen. For example, for the point κ , the two close nodes are n^1 and n^2 . Since $\mathbf{r} \times \mathbf{r}^2$ is positive (according to our convention), the node n^2 is chosen. Three curves pass through n^2 . The tangents of each curve are computed, and the angles between each of the tangents and that of the c^1 tangent are computed. The curve that yields the minimum angle is chosen (i.e., curve c^2). Two nodes on curve c^2 exist, namely, n^6 and n^3 . According to this convention, n^3 is chosen because it results in a positive normal when a cross-product is performed. The procedure is continued until the starting node is encountered. The procedure is used to trace other regions (subsurface) until all subsurfaces are traced. Similarly, all singular surfaces are intersected and partitioned into subsurfaces.

To determine whether each subsurface is a boundary or internal subsurface to the workspace, the perturbation method, eq. (44), is implemented. For example, consider the point $p^1(\mathbf{q})$ on the subsurface Ψ^1 which has the set of generalized coordinates $q_2 = 0.4$ and $q_3 = 3.4$. Note that

the subsurface Ψ^1 is defined as follows

$$\Psi^1 = \begin{bmatrix} 7.0711 \cos q_2 \cos q_3 \\ +7.0711(\sin q_3 - \sin q_2) \\ +14.1421 \cos q_2 \\ -7.0711 \cos q_2 \cos q_3 \\ +7.0711(\sin q_3 + \sin q_2) \\ -14.1421 \cos q_2 \\ 10 \cos q_2 \sin q_3 \\ +10 \cos q_2 \\ +20 \sin q_2 + 50 \end{bmatrix} \quad (70)$$

enclosed by the following boundary curve segments

$$\begin{aligned} c^1 &\text{ on the interval } [n^2 \ n^8] \\ c^3 &\text{ on the interval } [n^8 \ n^9] \\ c^4 &\text{ on the interval } [n^9 \ n^2] \end{aligned}$$

To determine the normal to Ψ^1 using eq. (43), partial derivatives representing tangent vectors are evaluated such that

$$\frac{\partial \Psi^1}{\partial q_2} = \begin{bmatrix} -7.07 \sin q_2 \cos q_3 - 7.07 \cos q_2 \\ -14.14 \sin q_2 \\ 7.07 \sin q_2 \cos q_3 + 7.07 \cos q_2 \\ +14.14 \sin q_2 \\ 10 \cos q_2 \cos q_3 - 10 \sin q_2 + 20 \cos q_2 \end{bmatrix} \quad (71)$$

and

$$\frac{\partial \Psi^1}{\partial q_3} = \begin{bmatrix} -7.07 \cos q_2 \sin q_3 + 7.07 \cos q_3 \\ 7.07 \cos q_2 \sin q_3 + 7.07 \cos q_3 \\ -10 \sin q_2 \sin q_3 \end{bmatrix} \quad (72)$$

The normal is computed

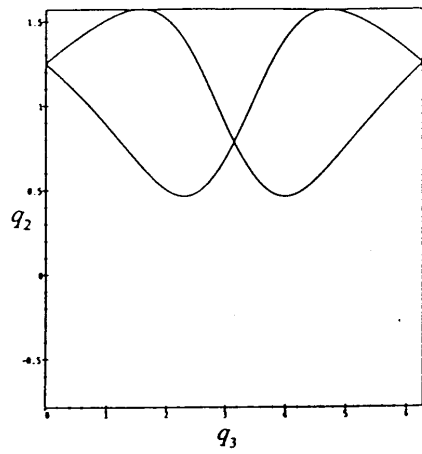
$$\mathbf{n} = \frac{\partial \Psi^1}{\partial q_2} \times \frac{\partial \Psi^1}{\partial q_3} = \begin{bmatrix} \frac{707}{-10}(\cos q_2(\cos q_3)^2 - \sin q_3 \cos q_3) \\ -\sin q_3 + \sin q_2 \cos q_3 - 2 \cos q_2 \cos q_3 \\ \frac{707}{-10}(\cos q_3 \sin q_2 + \cos q_2(\cos q_3)^2) \\ -2 \sin q_3 - \cos q_3 \sin q_2 + \cos q_2 \cos q_3 \\ \frac{499849}{-5000}(\sin q_2 \cos q_3 - \cos q_2 \cos q_3) \\ -\sin q_2(\cos q_3)^2 \end{bmatrix} \quad (73)$$

The unit normal $\hat{\mathbf{n}} = \mathbf{n}/\|\mathbf{n}\|$ at the point \mathbf{q}^0 on the subsurface Ψ^1 is evaluated

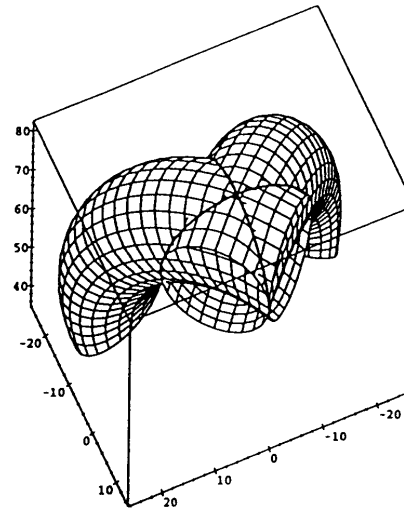
$$\hat{\mathbf{n}} = \mathbf{n}/\|\mathbf{n}\| = [0.098 \ -0.452 \ 0.887]^T \quad (74)$$

For a small perturbation $\partial \varepsilon = +0.1$, the coordinates of the perturbed point are computed as

$$\mathbf{x} = \Psi^i(\mathbf{q}^0) + \partial \varepsilon \hat{\mathbf{n}}(\mathbf{q}^0) = [6.513 \ -1.812 \ 63.418]^T \quad (75)$$



(a)



(b)

Fig. 7. Resulting intersection curves between two singular surfaces.

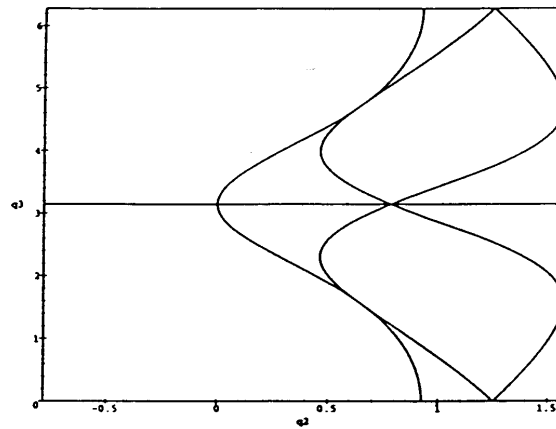


Fig. 8. Intersection curves dividing singular surface \mathbf{x}^1 into subsurfaces.

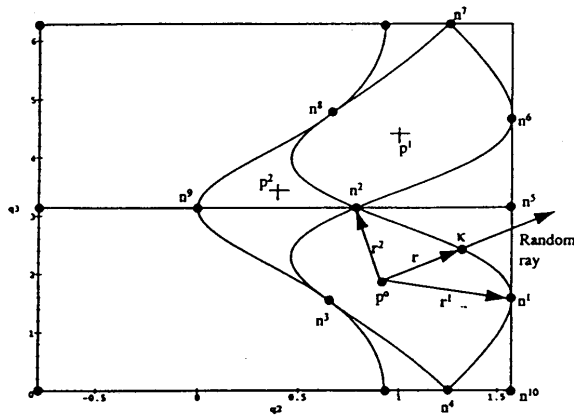


Fig. 9. Determining boundary segments for each subsurface.

Solving eq. (44) subject to the inequalities of eq. (45), there exists a solution such that the generalized set is $\mathbf{q} = [2.321 \ 1.222 \ -3.502]^T$. For a perturbation of $\partial\epsilon = -0.1$, the coordinates of the perturbed point are due to

$$\mathbf{x} = \Psi^i(\mathbf{q}^0) - \partial\epsilon \hat{\mathbf{n}}(\mathbf{q}^0) = [6.494 \ -1.721 \ 63.241]^T \quad (76)$$

and the solution for this position is the generalized set $\mathbf{q} = [2.393 \ 1.231 \ -3.463]^T$. Thus, both perturbation points are inside the workspace, which guarantees that this subsurface is internal. For subsurface Ψ^2 , the point on this subsurface is chosen as $p^2(\mathbf{q})$, which has coordinates $q_2 = 1.0$ and $q_3 = 4.4$. The unit normal $\hat{\mathbf{n}} = \mathbf{n}/\|\mathbf{n}\|$ at the point \mathbf{q}^0 on the subsurface Ψ^2 is evaluated as

$$\hat{\mathbf{n}} = \mathbf{n}/\|\mathbf{n}\| = [0.671 \ 0.653 \ 0.351]^T \quad (77)$$

For a small perturbation $\partial\epsilon = +0.1$, the coordinates of the perturbed point are

$$\mathbf{x} = \Psi^i(\mathbf{q}^0) + \partial\epsilon \hat{\mathbf{n}}(\mathbf{q}^0) = [-6.211 \ -7.245 \ 69.646]^T \quad (78)$$

For this perturbed point, a solution of eq. (44) subject to the inequality constraints of eq. (45) can be found such that the set of generalized coordinates is $\mathbf{q} = [2.276 \ 1.114 \ 1.882]^T$. A solution, however, cannot be found for $-\partial\epsilon$. This indicates that Ψ^2 is a boundary subsurface to the workspace.

Using this technique, boundary subsurfaces of each singular surface are determined. These surfaces are depicted in Figure 10 (in two different views). The volume enclosed by these surfaces is the workspace.

The above method was used to determine the boundary of the workspace for a number of manipulator configurations. Figure (11) depicts workspace boundaries for a

variety of combinations of revolute (R) and prismatic (P) joints.

4. Conclusions

The formulation of a general 3-DOF manipulator workspace has been shown to be valid for manipulators with joint limits formed in terms of inequality constraints. No limitations on the types of joints have been set. Although the computations involve numerical techniques, the resultant surfaces bounding the workspace are analytically parameterized.

It has been shown that singular surfaces can be partitioned into subsurfaces. The boundaries of these subsurfaces are defined by determining singular curves that result from the intersection of two singular surfaces. Subsurfaces can be entirely on the boundary of the workspace, or entirely inside the workspace. Difficulties in computing second-order singularities may arise when similar parametric surfaces are encountered. A technique for computing a tangent at the intersection of two singular surfaces has been presented. Since singular curves are computed numerically using marching methods, difficulties in parameterizing these curves occurred. The authors are in the process of developing a method to parameterize singular curves, as well as to automatically select a point on the subsurface via computing the centroid.

This work is currently being expanded to higher degrees of freedom by segmenting a manipulator to a number of three-degree-of-freedom systems. The envelope of one segment while inside the workspace of another segment is traced.

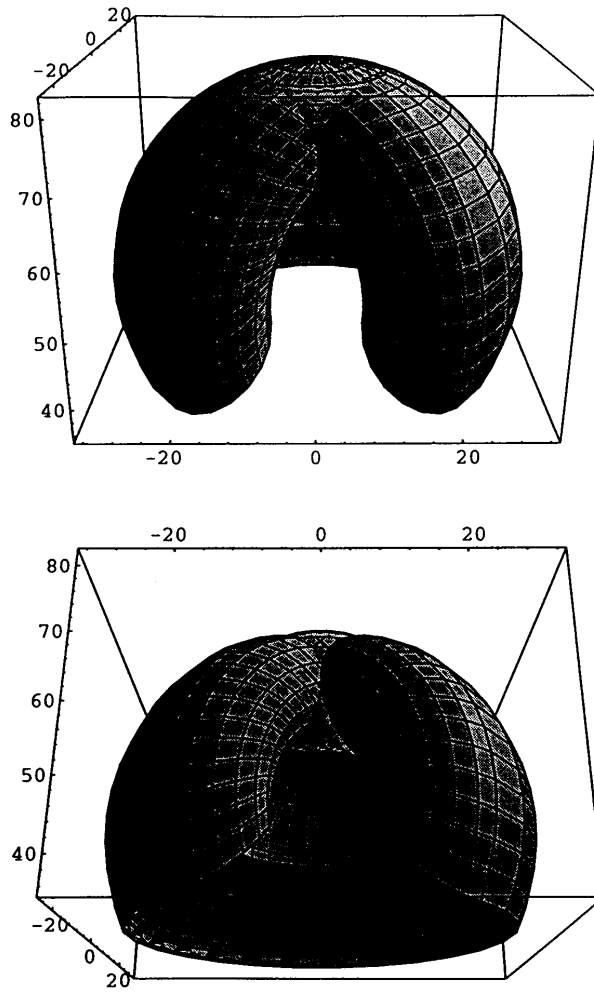


Fig. 10. Analytical surfaces that are boundary to the workspace.

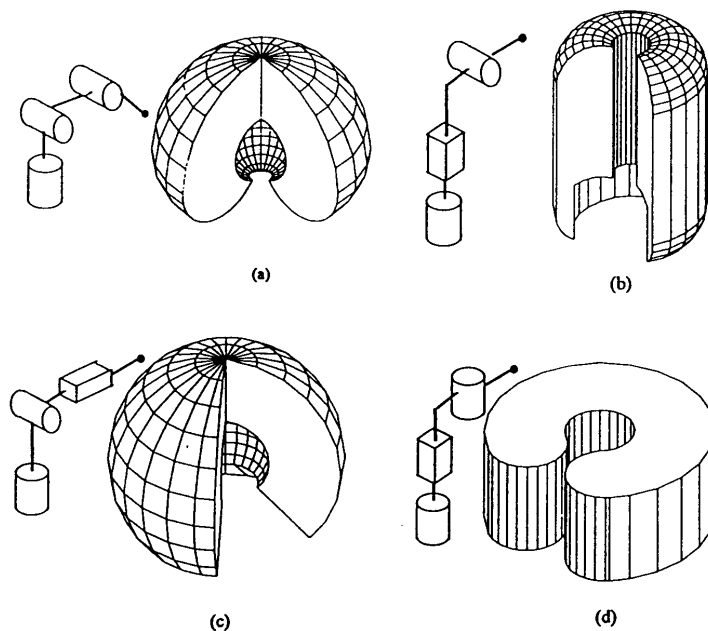


Fig. 11. Workspace of (A) RRR, (B) RPR, (C) RRP, (D) RPR.

References

- Abdel-Malek, K. 1995. Dexterity of manipulator arms at an operating point. *Proc. 21st Advances in Design Automation Conf.*, Vol. 82(1). ASME, pp. 781-788.
- Agrawal, S. K. 1990. Workspace boundaries of in-parallel manipulator systems. *Int. J. Robot. Automat.* 7(2):94-99.
- Allgower, E. L., and Georg, K. 1990. *Numerical Continuation Methods: An Introduction*. Berlin: Springer-Verlag.
- Cecarelli, M., and Vinciguerra, A. 1995. On the workspace of general 4R manipulators. *Int. J. Robot. Res.* 14(2):152-160.
- Denavit, J., and Hartenberg, R. S. 1955. A kinematic notation for lower-pair mechanisms based on matrices. *J. Appl. Mech.* 22:215-221.
- Emiris, D. M. 1993. Workspace analysis of realistic elbow and dual-elbow robot. *Mech. Machine Theory* 28(3):375-396.
- Gosselin, C., and Angeles, J. 1990. Singularity analysis of closed loop kinematic chains. *IEEE Trans. Robot. Automat.* 6(3):281-290.
- Gupta, K. G., and Roth, B. 1982. Design considerations for manipulator workspace. *J. Mech. Des.* 104(4):704-711.
- Haug, E. J., Adkins, R., and Luh, C. M. 1994. Numerical algorithms for mapping boundaries of manipulator workspaces. *Proc. 23rd ASME Mechanisms Conf.* (Minneapolis, MN).
- Haug, E. J., Wang, J. Y., and Wu, J. K. 1992. Dexterous workspaces of manipulators: I. analytical criteria. *Mech. Struct. Mach.* 20(3):321-361.
- Keller, H. B. 1987. *Lectures on Numerical Methods in Bifurcation Problems*. Berlin: Springer-Verlag.
- Kleinfinger, J. F. 1986. *Modélisation dynamique de robots a chaîne cinématique simple, arborescente ou fermée, en vue de leur commande*. Ph.D. thesis, Université de Nantes.
- Kumar, V. 1985. Robot Manipulators—Workspaces and Geometric Dexterity. Master's thesis, Ohio State University.
- Kumar, A., and Waldron, K. J. 1981. The dexterous workspace. ASME Special Paper 80-DET.
- Lai, Z. C. 1986. On the Dexterity of Robotic Manipulators. Ph.D. dissertation, University of California, Los Angeles, CA.
- Lai, Z. C., and Menq, C. 1988. The dexterous workspace of simple manipulators. *IEEE J. Robot. Automat.* 4(1):99-103.

- Lucaks, G. 1990. Simple singularities in surface-surface intersections. In Gregory, J. A., (ed.), *The Mathematics of Surfaces*. Oxford: Clarendon Press.
- McKerrow, P. J. 1991. *Introduction to Robotics*. Reading, MA: Addison-Wesley.
- Muellenheim, G. 1991. On determining start points for a surface/surface intersection algorithm. *Computer Aided Geometric Design* 8(5):401-408.
- Nutbourne, A. N., and Martin, R. R. 1988. *Differential Geometry Applied to Curve and Surface Design, Volume 1: Foundations*. Chichester, UK: Ellis Horwood.
- Pennock, G. R., and Kassner, D. J. 1993. The workspace of a general planar three-degree-of-freedom platform-type manipulator. *ASME J. Mech. Des.* 115(2):269-276.
- Pratt, M. J., and Geisow, A. D. 1986. Surface/surface intersection problems. In Gregory, J. A., (ed.), *The Mathematics of Surfaces*. Oxford: Clarendon Press.
- Qiu, C. C., Luh, C. M., and Haug, E. J. 1995. Dexterous workspaces of manipulators, part III: calculation of continuation curves at bifurcation points. *Mechanics of Structures and Machines* 23(1):115-130.
- Qiulin, D., and Davies, B. J. 1987. *Surface Engineering Geometry for Computer-Aided Design and Manufacturing*. Hampstead, UK: Ellis Horwood.
- Rheinboldt, W. C. 1986. *Numerical Analysis of Parameterized Nonlinear Equations*. New York: John Wiley and Sons.
- Roth, B. 1975. Performance evaluation of manipulators from a kinematic viewpoint. National Bureau of Standards Special Publications no. 459, pp. 39-61.
- Tsai, Y. C., and Soni, A. H. 1981. Accessible region and synthesis of robot arm. ASME special paper 80-DET-101, pp. 803-811.
- Vinogradov, I. et. al. 1971. Details of kinematics of manipulators with the method of volumes. (Russian). *Mexanika Mashin* No. 27/28: 5-16.
- Wang, J. Y., and Wu, J. K., 1993. Dexterous workspaces of manipulators, part 2: computational methods. *Mech. Structures and Machines* 21(4):471-506.
- Wilf, I., and Manor, Y. 1993. Quadric-surface intersection curves: shape and structure. *Computer Aided Design* 25(10):633-643.
- Yang, D. C. H., and Lai, Z. C. 1985. On the dexterity of robotic manipulators-service angle. *Trans. ASME J. Mech. Transm. Automat. Design* 107(2):262-270.
- Yang, D. C. H., and Lee, T. W. 1983. On the workspace of mechanical manipulators. *J. Mech. Trans. Automat. Design* 105(1):62-69.